Synthesis and structure of novel lithium-ion conductor $Li_7Ge_3PS_{12}$

Yuki Inoue[a], Kota Suzuki[a,b], Naoki Matsui[a], Masaaki Hirayama[a,b], Ryoji Kanno[a,b,*]

[a] *Department of Electronic Chemistry, Interdisciplinary Graduate School of Science and Engineering, Tokyo Institute of Technology, 4259 Nagatsuta, Midori, Yokohama 226-8502, Japan*
[b] *Department of Chemical Science and Engineering, School of Materials and Chemical Technology, Tokyo Institute of Technology, 4259 Nagatsuta, Midori, Yokohama 226-8502, Japan*

A B S T R A C T

The novel lithium-ion conductor $Li_7Ge_3PS_{12}$ was synthesized by slow cooling from the ternary $Li_2S–GeS_2–P_2S_5$ system, and was shown to exhibit a cubic argyrodite-type structure. The phase composition was determined by varying the ratio of starting materials; the observed monophasic properties were close to those for the $Li_7Ge_3PS_{12}$ composition. The lattice parameter (a =9.80192(3) Å) of $Li_7Ge_3PS_{12}$ was slightly smaller than that of Li_7PS_6 (a =9.993 Å), indicating that substitution of a Li cation by the smaller Ge cation contracted the cubic lattice. In addition, the novel structure consisted of a framework composed of four isolated $(Ge/P)S_4$ tetrahedra. Li^+ ions occupied tetrahedral sites within the framework, forming a three-dimensional conduction pathway. Finally, $Li_7Ge_3PS_{12}$ exhibited a high ionic conductivity of 1.1×10^{-4} S cm^{-1} at 25 °C and an activation energy of 25 kJ mol^{-1}.

1. Introduction

Lithium-ion conductors are of great interest for use as solid electrolytes in lithium-ion batteries, as they have the potential to allow operation under significantly more severe conditions than those suitable for current battery systems [1,2]. In particular, the development of stable and non-flammable electrolytes could improve battery reliability, with solid electrolytes being promising candidates for this purpose. However, a number of issues remain, including the search for novel solid electrolytes exhibiting high lithium-ion conductivity combined with high electrochemical and chemical stabilities [2–5]. Thus, the discovery and development of new lithium-ion conducting solids is important to provide additional materials for all-solid-state battery systems.

One example of a crystalline superionic conductor is $Li_{10}GeP_2S_{12}$, which exhibits an extremely high lithium-ion conductivity of 1.2×10^{-2} S cm^{-1} at 27 °C and a high electrochemical stability > 5 V versus lithium [1]. This material exists in the $Li_2S–GeS_2–P_2S_5$ system, which also includes a number of other lithium-ion conductors with high ionic conductivities. Examples include $Li_4GeS_4–Li_3PS_4$ solid solutions with the LISICON-type structure [6,7], Li_7PS_6 with the argyrodite-type structure [8,9], and $Li_7P_3S_{11}$ glass ceramics [10]. Indeed, previous reports have indicated that this quasi-ternary system could provide various novel materials exhibiting high lithium-ion conducting characteristics, with a number of materials potentially remaining unexplored.

Among the various ionic conductors reported to date, materials exhibiting an argyrodite-type structure can be considered interesting candidates because they allow anion/cation substitution in their crystal structure [11]. The term *argyrodite* is derived from the mineral Ag_8GeS_6. Various atomic substitutions in the structure of this mineral have provided a wide range of argyrodite-type materials suitable for the ionic conduction of monovalent cations, including Ag^+ and Cu^+ [12,13]. However, to date, only a few argyrodite-type materials had been reported as lithium-ion conductors in the anion/cation substituted Li_7PS_6 system. For example, halogen-substituted compounds such as Li_6PS_5X (X = Cl, Br, I) have cubic argyrodite-type structures and exhibit a lithium-ion conductivity of 10^{-4} S cm^{-1} at room temperature [14,15]. The argyrodite structure consists of 136 tetrahedral sites in a unit cell, including four isolated PS_4 tetrahedra in a tetrahedrally close-packed anion array, in which 24 lithium ions occupy sites within the remaining 132 empty tetrahedral sites [11]. This distribution of lithium ions, which contributes to ionic diffusion, is characteristic of the argyrodite structure.

Thus, we herein report the development of a novel lithium-ion conducting crystalline material, focusing on the ternary $Li_2S–GeS_2–P_2S_5$ system, examining a previously un-synthesized composition. A systematic materials search will be carried out to identify any novel crystalline materials, and the relationship between structure and ionic conductivity will be investigated.

Table 1
Reaction products detected in the prepared Li_2S–GeS_2–P_2S_5 system.

Sample Number	Mole fraction in starting material			Identified phases
	Li_2S	GeS_2	P_2S_5	
1	0.63	0.09	0.27	$Li_4P_2S_6$, GeS_2, unknown[a]
2	0.62	0.25	0.13	Li_3PS_4, GeS_2, unknown[a]
3	0.61	0.33	0.06	Li_4GeS_4, GeS_2, unknown[a]
4	0.6	0.16	0.24	$Li_4P_2S_6$, GeS_2, unknown[a]
5	0.5	0.2	0.3	$Li_4P_2S_6$, GeS_2
6	0.5	0.33	0.17	$Li_4P_2S_6$, GeS_2, unknown[a]
7	0.5	0.38	0.12	Argyrodite[c], $Li_4P_2S_6$, GeS_2, unknown[a]
8	0.51	0.42	0.07	Argyrodite[c], $Li_4P_2S_6$
9[b]	0.5	0.43	0.07	Argyrodite[c], $Li_4P_2S_6$
10	0.49	0.44	0.07	Argyrodite[c], $Li_4P_2S_6$
11	0.46	0.47	0.07	Argyrodite[c], $Li_4P_2S_6$, GeS_2
12	0.48	0.47	0.06	Argyrodite[c], $Li_4P_2S_6$, GeS_2, unknown[a]
13	0.48	0.42	0.1	Argyrodite[c], $Li_4P_2S_6$, GeS_2
14	0.46	0.46	0.09	Argyrodite[c], $Li_4P_2S_6$, GeS_2
15	0.44	0.49	0.07	Argyrodite[c], $Li_4P_2S_6$, GeS_2
16	0.41	0.52	0.07	GeS_2, unknown[a]
17	0.33	0.33	0.34	$Li_4P_2S_6$, GeS_2

Italic characters represent the main phase for each composition.

[a] Unknown = unidentified phases.

[b] Composition of number 9 is $Li_7Ge_3PS_{12}$.

[c] Argyrodite = a phase exhibiting an argyrodite-type structure.

2. Materials and methods

The starting materials, Li_2S (99.9%, Nippon Chemical Industrial Co. Ltd.), GeS_2 (> 99.99%, Kojundo Chemical Laboratory Co. Ltd.), and P_2S_5 (99%, Sigma-Aldrich), were mixed in the appropriate molar ratios (see Table 1) in an Ar-filled glovebox. All mixtures were pelletized, placed into carbon-coated quartz glass tubes, and sealed in a ~10 Pa vacuum. The samples were then heated at 870 °C for 8 h in a furnace and cooled slowly to 28 °C. The reaction products were characterized by powder X-ray diffraction under an argon atmosphere using a Rigaku SmartLab powder X-ray diffractometer with Cu Kα radiation (45 kV, 200 mA). The diffraction data were collected at 25 °C in a 2θ range of 10–120° with a step width of 0.01°.

The synchrotron X-ray diffraction pattern of the powdered sample was obtained at 25 °C using a Debye-Scherrer camera with an imaging plate at the BL02B2 beam line, at a wavelength of 0.6 Å. All measurements were carried out at the SPring-8 facility. Synchrotron X-ray diffraction data were analyzed using the Rietveld method and the RIETAN-FP package [16].

Ionic conductivity was determined using an alternating current (ac) impedance method in the frequency range of 1–1 MHz using a Solartron 1260 frequency response analyzer. A disk-shaped sample

(thickness: ~1 mm, diameter: ~6 mm) was prepared for conductivity measurements by solidifying the melt above the melting point of the material (~570 °C). Gold paste electrodes were coated on the surfaces of the disk prior to heating under vacuum at 150 °C for 3 h. The data were collected under a flow of Ar gas between 25 and 105 °C. Differential thermal analysis (DTA) was performed using a Rigaku Thermo Plus TG 8120 system between 24 and 900 °C for the sample sealed in an evacuated quartz ampule.

The charge and discharge characteristics of the all-solid-state battery were examined using $Li_7Ge_3PS_{12}$ as a solid electrolyte. The positive and negative electrodes were composed of a mixture of $LiNbO_3$-coated $LiCoO_2$ and Li-In metal (thicknesses: 0.3 mm (Li) and 0.1 mm (In), diameters: 10 mm (Li and In)) [17]. The electrochemical properties of the cell were determined using a TOSCAT-3100 battery analyzer (Toyo System Co. Ltd.). A cycling test was carried out between 1.9 and 3.6 V (*vs.* Li-In: ~0.6 V *vs.* Li/Li$^+$) at an applied current of 7.25 mA g^{-1} at 25 °C.

3. Results and discussion

A materials search for lithium-ion conductors was carried out using the formation diagram of the quasi-ternary Li_2S–GeS_2–P_2S_5 system, which is depicted in Fig. 1. In this system, intermediate crystalline compounds, such as Li_3PS_4 (thio-LISICON structure) [18], Li_7PS_6 (argyrodite structure) [9], and $Li_7P_3S_{11}$[10] exist in the Li_2S–P_2S_5 tie line, while Li_4GeS_4[19–22] and the $Li_{10}GeP_2S_{12}$-type $Li_{4-k}Ge_{1-k}P_kS_4$ solid-solution exist in the Li_3PS_4–Li_4GeS_4 tie line [1,7,23]. Although other compositions have also been reported [24,25], large regions of the diagram remain unexamined. Table 1 summarizes the compositions synthesized herein along with the phase identification results obtained from X-ray diffraction measurements. For clarity, all compositions are numbered consistently throughout Figs. 1 and 2. A number of X-ray diffraction patterns of the materials synthesized in the ternary system are provided in Fig. 2, which shows that the observed phases were indexed as GeS_2, $Li_4P_2S_6$, Li_3PS_4, and Li_4GeS_4, together with peaks corresponding to the new argyrodite phase. Specific analysis close to the region of formation of the new phase indicated that this novel phase could be generated with a nominal composition close to that of $Li_7Ge_3PS_{12}$ (see composition number 9 in Table 1).

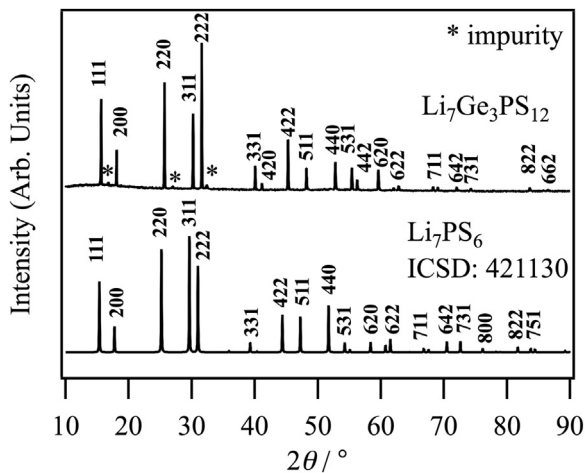Fig. 3 shows the X-ray diffraction patterns of both $Li_7Ge_3PS_{12}$ and the cubic high-temperature modification of Li_7PS_6 with the F-43m space group (no. 216) (ICSD no. 421130) exhibiting an argyrodite-type structure. The two diffraction patterns are similar, indicating that the novel $Li_7Ge_3PS_{12}$ phase also exhibits a cubic argyrodite-type structure. The diffraction peaks of this new phase were indexed assuming a cubic unit cell with an F-43m space group. Interestingly, the shifts of a number of peaks to higher angles compared to the Li_7PS_6 pattern indicate that the new phase contains smaller lattice parameters.
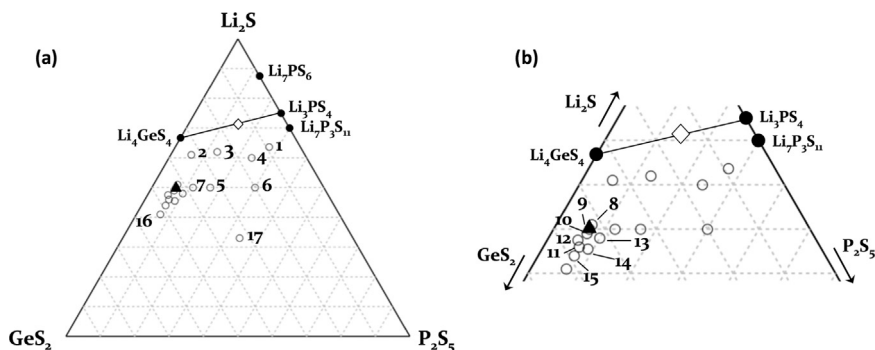
Fig. 1. Formation diagram of the Li_2S-GeS_2-P_2S_5 quasi-ternary system. (a) The full Li_2S-GeS_2-P_2S_5 region, and (b) the region close to the new argyrodite type phase (▲: #9) discovered in this study. Numbered hollow circles (○) indicate the compositions synthesized in this study. The numbers correspond to those used in the XRD patterns (Fig. 2) and in the composition table (Table 1). Bold circles (•) indicate previously reported compositions for this system, and hollow diamonds (◇) depict the composition of the $Li_{10}GeP_2S_{12}$ superionic conductor on the tie line of Li_4GeS_4 and Li_3PS_4.
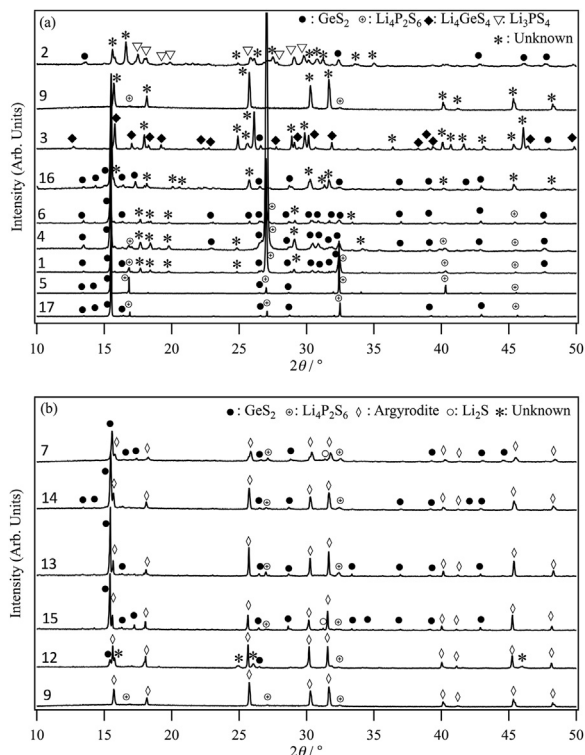
Fig. 2. (a) Representative X-ray diffraction patterns of the materials synthesized in the Li_2S-GeS_2-P_2S_5 system, and (b) X-ray diffraction patterns of the materials with compositions close to that of $Li_7Ge_3PS_{12}$ (#9). Dominant diffraction lines are labeled according to phases with the following structures: Li_2S, GeS_2, $Li_4P_2S_6$, Li_4GeS_4, Li_3PS_4, argyrodite, and unknown.

Fig. 3. X-ray diffraction patterns of the novel argyrodite-type phase with $Li_7Ge_3PS_{12}$ composition, and of the previously reported argyrodite-type Li_7PS_6 (ICSD: 421130).

Moreover, the additional signals could be assigned to $Li_4P_2S_6$[26], indicating the presence of small amounts of this impurity phase.

The crystal structure of the new phase was determined using synchrotron X-ray diffraction data of the powdered $Li_7Ge_3PS_{12}$ sample at 25 °C. A two-phase model based on $Li_7Ge_3PS_{12}$ argyrodite (space group: F-$43m$) and $Li_4P_2S_6$ (space group: $P63/mcm$) as the main phase and second impurity phase, respectively, was used for the refinement. The initial parameters for the Rietveld refinement of Li_7PS_6 were also employed for the novel material, i.e., space group F-$43m$ (no. 216), Li at 48 h, P at 4b, and S at 16e, 4a, and 4c sites [27]. Since $Li_7Ge_3PS_{12}$ has a larger number of multivalent cations in its structure, the positions of P and Ge were initially examined for both the 48 h and 4b sites. Indeed, the refinement provided a good reliability factor assuming that both Ge and P occupy the original position of the P 4b site in the cubic argyrodite-type structure. In addition, the Li and Ge components were refined at the original Li positions of the 48 h site. The final refinement and structural parameters are summarized in Table 2, and the interatomic distances and bond angles are outlined in Table 3. Furthermore, the refinement pattern is shown in Fig. 4. From these results, we determined that the two-phase model provided a good fitting, with an R_{wp} value of 2.45%.

Fig. 5 shows the structure of the argyrodite-type $Li_7Ge_3PS_{12}$ structure determined using the above refinement results. This new phase adopts a cubic structure with a lattice parameter, a, equal to 9.78525(5) Å, which is smaller than that of Li_7PS_6 (a =9.993 Å). The structure is characterized by the ordered arrangement of four $(Ge/P)S_4$ tetrahedra, which contrasts to both the four PS_4 tetrahedra present in Li_7PS_6 and the anion substituted system observed for Li_6PS_5X (X = Cl, Br, I). In addition, lithium ions are distributed in the tetrahedral 48 h site, which exists in a bi-pyramidal structure formed by two LiS_4 tetrahedra connected through face sharing. Structural analysis indicated that Ge was also distributed in the 48 h site, with refinement results giving Li and Ge occupation parameters in the 48 h site of 0.42 and 0.08, respectively. In addition, the (Ge/P)-S bond distance (i.e., 2.093 Å) in the $(Ge/P)S_4$ tetrahedra of $Li_7Ge_3PS_{12}$ is larger than that in Li_7PS_6 (i.e., 2.042 Å), which is consistent with the difference in the ionic radii between P and Ge (ionic radii: Li(C.N.4) =0.59 Å; Ge(C.N.4) =0.39 Å; P(C.N.4) =0.17 Å). Furthermore, the Li-S distance of 2.41–2.52 Å in the LiS_4 tetrahedra of $Li_7Ge_3PS_{12}$ is shorter than that of Li_7PS_6 (i.e., 2.45–2.59 Å), which indicates substitution of the smaller Ge ion at the Li 48 h site. To the best of our knowledge, this is the first report to demonstrate the co-existence of Ge with Li at the center of tetrahedral sites in sulfide compounds. The contracted bond length between (Li/Ge) and S and the occupation parameter of Ge in the 48 h site (g(Ge)/[g(Li)+g(Ge)] =0.24) support the structural model with the partial distribution of Ge in Li sites. Although detailed structural analysis with neutron powder diffraction will be examined in the future, these structural changes are consistent with the lower lattice parameter for the novel Ge-substituted phase.

Fig. 6(a) shows the complex impedance plots (Nyquist plots) for $Li_7Ge_3PS_{12}$ measured at several temperatures between 25 and 105 °C. The spike shown in the plot corresponds to the electrode contribution,

Table 2
Structural parameters obtained from Rietveld refinement analysis of the synchrotron XRD data of $Li_7Ge_3PS_{12}$ using the F-$43m$ space group.

Atom	Site	g	x	y	z	B (Å²)
Li(1)	48 h	0.2884(9)	0.81875(19)	= x[Li(1)]	0.0140(4)	4.86 (13)
Ge(1)	48 h	= 0.375-g[Li(1)]	= x[Li(1)]	= x[Li(1)]	= z[Li(1)]	= B[Li(1)]
P(1)	4b	0.499(5)	1/2	1/2	1/2	1.95(3)
Ge(2)	4b	= 1-g[P(1)]	1/2	1/2	1/2	= B[P(1)]
S(1)	16e	1.0	0.62329(10)	= x[S(1)]	= x[S(1)]	5.71(6)
S(2)	4c	1.0	1/4	1/4	1/4	5.92(8)
S(3)	4a	1.0	0	0	0	7.11(9)

Unit cell: Cubic F-$43m$ (216); a =9.80192(3) Å, V =941.744(5) Å³; R_{wp} =2.45%, R_e =2.19%, R_p =1.40%, R_b =2.67%, R_F =2.70%, goodness of fit $S = R_{wp}/R_e$ =1.12; secondary phase: $Li_4P_2S_6$ (~2.4 mass%).

Table 3
Interatomic bond distances (Å) and angles (°) for $Li_7Ge_3PS_{12}$ (upper table) and Li_7PS_6 (lower table).

| (Ge/P)S$_4$ (Tetrahedra)		(Li/Ge)S$_4$ (Tetrahedra)	
(Ge/P)–S(1)[i]	2.0931(6)	(Li/Ge)–S(1)[i]	2.409(4)
(Ge/P)–S(1)[ii]	2.0931(6)	(Li/Ge)–S(1)[v]	2.4091(19)
(Ge/P)–S(1)[iii]	2.0931(6)	(Li/Ge)–S(2)	2.5021(11)
(Ge/P)–S(1)[iv]	2.0931(6)	(Li/Ge)–S(3)	2.516(3)
S(1)[i]–(Ge/P)–S(1)[ii]	109.47(4)	S(1)[i] –(Li/Ge)–S(1)[v]	93.62(8)
S(1)[i]–(Ge/P)–S(1)[iii]	109.47(4)	S(1)[i] –(Li/Ge)–S(2)	111.45(9)
S(1)[i]–(Ge/P)–S(1)[iv]	109.47(4)	S(1)[i] –(Li/Ge)–S(3)	111.38(13)
S(1)[ii]–(Ge/P)–S(1)[iii]	109.47(4)	S(1)[v]–(Li/Ge)–S(2)	111.45(15)
S(1)[ii]–(Ge/P)–S(1)[iv]	109.47(4)	S(1)[v]–(Li/Ge)–S(3)	111.38(9)
S(1)[iii]–(Ge/P)–S(1)[iv]	109.47(4)	S(2)–(Li/Ge)–S(3)	115.51(7)
PS$_4$ (Tetrahedra)		LiS$_4$ (Tetrahedra)	
P–S(1)[i]	2.04231	Li– S(1)[i]	2.53041
P–S(1)[ii]	2.04231	Li– S(1)[v]	2.53041
P–S(1)[iii]	2.04231	Li–S(2)	2.45152
P–S(1)[iv]	2.04231	Li–S(3)	2.59016
S(1)[i]–P–S(1)[ii]	109.4712	S(1)[i]–Li–S(1)[v]	94.9845
S(1)[i]–P–S(1)[iii]	109.4712	S(1)[i]–Li–S(2)	111.7088
S(1)[i]–P–S(1)[iv]	109.4712	S(1)[i]–Li–S(3)	108.8705
S(1)[ii]–P–S(1)[iii]	109.4712	S(1)[v]–Li–S(2)	111.7088
S(1)[ii]–P–S(1)[iv]	109.4712	S(1)[v]–Li–S(3)	108.8705
S(1)[iii]–P–S(1)[iv]	109.4712	S(2)–Li–S(3)	118.2112

Symmetry codes: (i) x, y, z; (ii) $-z, -y, x$; (iii) $-z, y, -x$; (iv) $z, -y, -x$ (v) $-z+1/2, y, -x+1/2$.
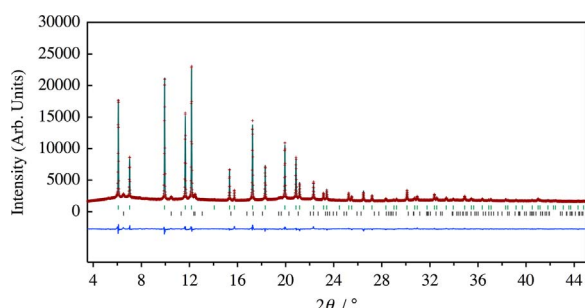
Fig. 4. Synchrotron X-ray Rietveld refinement patterns for $Li_7Ge_3PS_{12}$. Observed data points are indicated by cross marks (+). Solid lines overlaying the data were obtained via Rietveld refinement. Vertical markers below the patterns indicate the positions of possible Bragg reflections of the F-$43m$ space group for the argyrodite-type (green) and the impurity $Li_4P_2S_6$ (grey) phases. Differences between the observed and calculated intensities are plotted below the data on the same scale (blue line). (For interpretation of the references to color in this figure legend, the reader is referred to the web version of this article.)

the intercept of the extrapolated straight line with the x-axis (i.e., the Z' value at $Z'' = 0$) corresponds to the sum of the bulk and grain boundary contributions of the samples, and the ionic conductivity could be calculated as the sum of the bulk and grain boundary resistance values. Indeed, our material exhibited similar behavior to previously reported solid-sulfide lithium-ion conductors [23]. In addition, the temperature dependence of the $Li_7Ge_3PS_{12}$ conductivity is shown in Fig. 6(b). The conductivity value for the new material at 25 °C was determined to be 1.1×10^{-4} S cm^{-1}, which is high compared to that of Li_6PS_5X (X = Cl, Br, I) (i.e., 10^{-7}–10^{-4} S cm^{-1}) [15]. Furthermore, the high ionic conductivity could be attributed to the disordered arrangement of lithium ions within the structure, which is characteristic of argyrodite-type lithium-ion conductors (see Table 4) [15]. As indicated, the conductivity of $Li_7Ge_3PS_{12}$ is comparable to that of fast lithium-ion conductors, such as Li_6PS_5X (X = Cl, Br). Moreover, the activation energy during the heating process was calculated to be 25 kJ mol^{-1} at 25−100 °C, which is lower than that of Li_7PS_6 (i.e., 32 kJ mol^{-1}) [8]. Based on synchrotron XRD data, the presence of amorphous and $Li_4P_2S_6$ impurities was also indicated in addition to the main
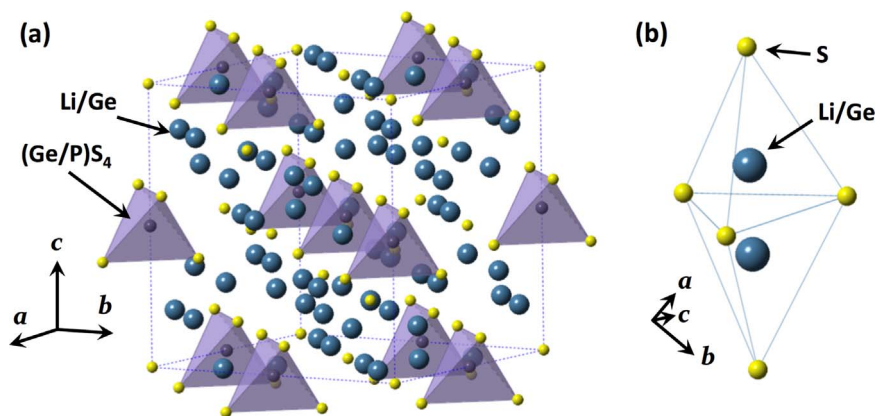
Fig. 5. (a) Crystal structure of the argyrodite-type $Li_7Ge_3PS_{12}$ structure as determined by Rietveld analysis. Yellow and blue spheres correspond to sulfur and to (Li/Ge) atoms, respectively. Purple tetrahedra represent the (Ge/P)S$_4$ units. (b) The coordination environment of the (Li/Ge)S$_4$ tetrahedra. Lithium atoms occupy the tetrahedral 48 h site with an occupation parameter of ~0.3. The tetrahedra form bi-pyramidal structures with face sharing connections. (For interpretation of the references to color in this figure legend, the reader is referred to the web version of this article.)

(a)

(b)
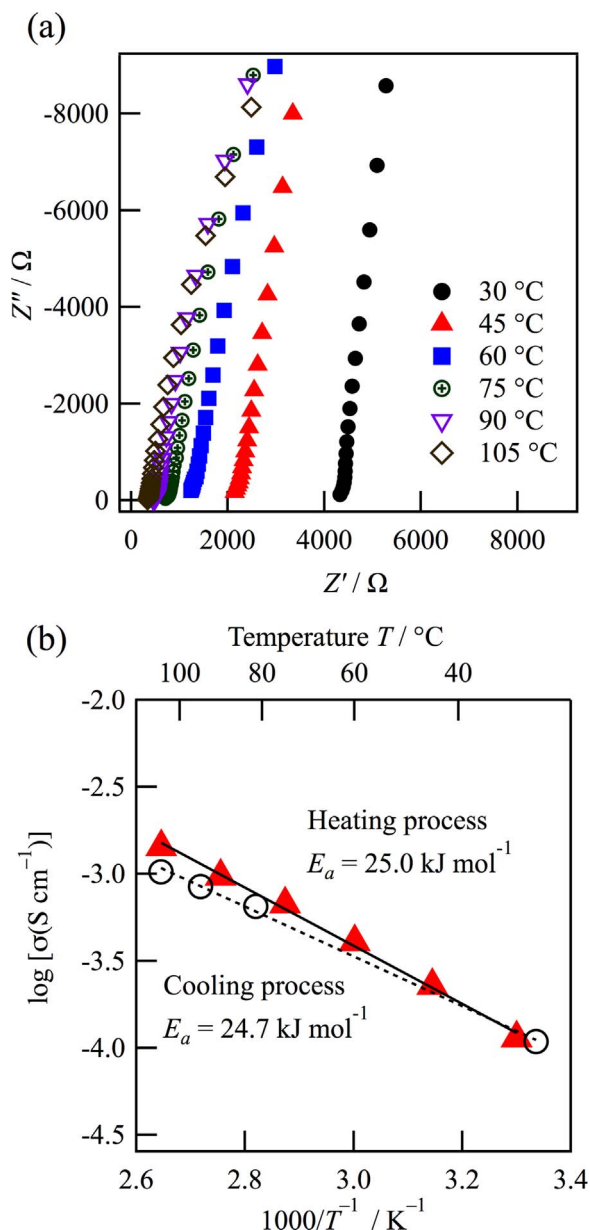
Fig. 6. (a) Nyquist plots at various temperatures for Li$_7$Ge$_3$PS$_{12}$ during the heating process, and (b) Arrhenius plots generated using the obtained impedance data. Bold red triangles (▲) and hollow black circles (○) indicate the ionic conductivity during heating and cooling, respectively. The activation energies of each process are also indicated. (For interpretation of the references to color in this figure legend, the reader is referred to the web version of this article.)

Li$_7$Ge$_3$PS$_{12}$ phase. The quantity of Li$_4$PS$_6$ was estimated to be ~2.4 wt. %, and this phase had a low ionic conductivity of 2.4×10^{-7} S cm^{-1} as reported previously [28]. The contribution of the non-crystalline phase to the observed high ionic conductivity was confirmed by measuring the conductivity of the pure non-crystalline phase synthesized by quenching the mixture of the same composition with Li$_7$Ge$_3$PS$_{12}$ from 950 °C. In this case, the conductivity of the glass sample was estimated to be ~10^{-6} S cm^{-1}. In addition, the conductivity of Li$_7$Ge$_3$PS$_{12}$ (i.e., 1.1×10^{-4} S cm^{-1}) was higher than those of both Li$_4$PS$_6$ and the non-crystalline phases by two or three orders of magnitude. Therefore, the observed conductivity for the mixture was mainly attributed to the intrinsic properties of the crystalline Li$_7$Ge$_3$PS$_{12}$, as the single Li$_7$Ge$_3$PS$_{12}$ phase is expected to exhibited higher conductivity than 1.1×10^{-4} S cm^{-1}.

However, the activation energy for ionic conduction in Li$_7$Ge$_3$PS$_{12}$ is significantly higher than those of Li$_6$PS$_5$X (X = Cl, Br), despite the similarities between the lattice sizes, thus indicating that the ionic conduction mechanism of Li$_7$Ge$_3$PS$_{12}$ differs from that of Li$_6$PS$_5$X (X = Cl, Br). Although the high ionic conductivity of Li$_6$PS$_5$X (X = Cl, Br) is due to the disordered arrangement of S^{2-} and X$^-$ ions in the structure, it appears that the high ionic conductivity of Li$_7$Ge$_3$PS$_{12}$ is attributed to the distribution of cations within the structure, and in particular the distribution of Li$^+$ ions. Thus, determination of the detailed cation distribution in the structure by neutron diffraction studies will allow the ionic conduction mechanism of Li$_7$Ge$_3$PS$_{12}$ to be elucidated.

Fig. 7 shows the DTA curves of Li$_7$Ge$_3$PS$_{12}$ during heating and cooling, and the XRD patterns recorded both before and after the DTA measurements are also shown. During heating, exothermic and endothermic peaks were observed at 450 and 570 °C, respectively. The exothermic peak is generally caused by a transformation from a metastable to a stable phase upon heating, which suggests that the Li$_7$Ge$_3$PS$_{12}$ is in a metastable state at low temperatures. The series of endothermic peaks at ~550 and 570 °C correspond to a phase transition to the low-temperature phase of Li$_7$Ge$_3$PS$_{12}$ and the melting of the phase, respectively. In the cooling cycle, the liquid-solid phase transition was confirmed at 520 °C, with crystallization at 500 °C being indicated by an exothermic peak. In addition, a small endothermic peak was observed at 370 °C in the cooling cycle, which was assigned to the phase transition from a metastable phase to a stable phase. From the XRD measurements following DTA, no clear change in crystal structure was observed, which indicates that the reaction kinetics of the metastable (high temperature) to stable (low temperature) phase transition were particularly low. The phase relationship around the low- and high-temperature phases will be elucidated in further studies.

The all-solid-state battery properties were then examined using Li$_7$Ge$_3$PS$_{12}$, Li-In, and LiNbO$_3$-coated LiCoO$_2$/Li$_{10}$GeP$_2$S$_{12}$ as the electrolyte, anode, and cathode materials, respectively. Fig. 8 shows the charge-discharge curves of the cell at 25 °C. The plateau regions of the charge curves at approximately 3.4 V likely correspond to the lithium extraction/insertion reaction of LiCoO$_2$. In addition, the cells exhibited an initial discharge capacity of ~80 mAh g^{-1}, which is slightly smaller than capacities reported for all-solid-state batteries containing

Table 4
Ionic conductive properties and structural parameters for the argyrodite-type lithium-ion conductors.

Composition	Ionic Conductivity σ/10^{-6} S cm^{-1}	Activation Energy E_a / kJ mol^{-1}	Lattice parameter a /Å	Bond distance d /Å		Ref.
				Li–S	P–S	
Li$_7$Ge$_3$PS$_{12}$	110 (300 K)	25	9.802	2.409(4)	2.0931(6)	–
Li$_6$PS$_5$Cl	740 (r.t.)	11	9.850	2.4833	2.0395	15
Li$_6$PS$_5$Br	720 (r.t.)	16	9.980	2.5222	2.0489	15
Li$_6$PS$_5$I	0.46 (r.t.)	24	10.142	2.6635	2.0459	15
HT-Li$_7$PS$_6$	30 (573 K)	34	9.993	2.5256	2.0423	8
LT-Li$_7$PS$_6$	1.6 (313 K)	15	–	–	–	8

HT and LT indicate high-temperature and low-temperature modifications of the crystal structures, respectively.
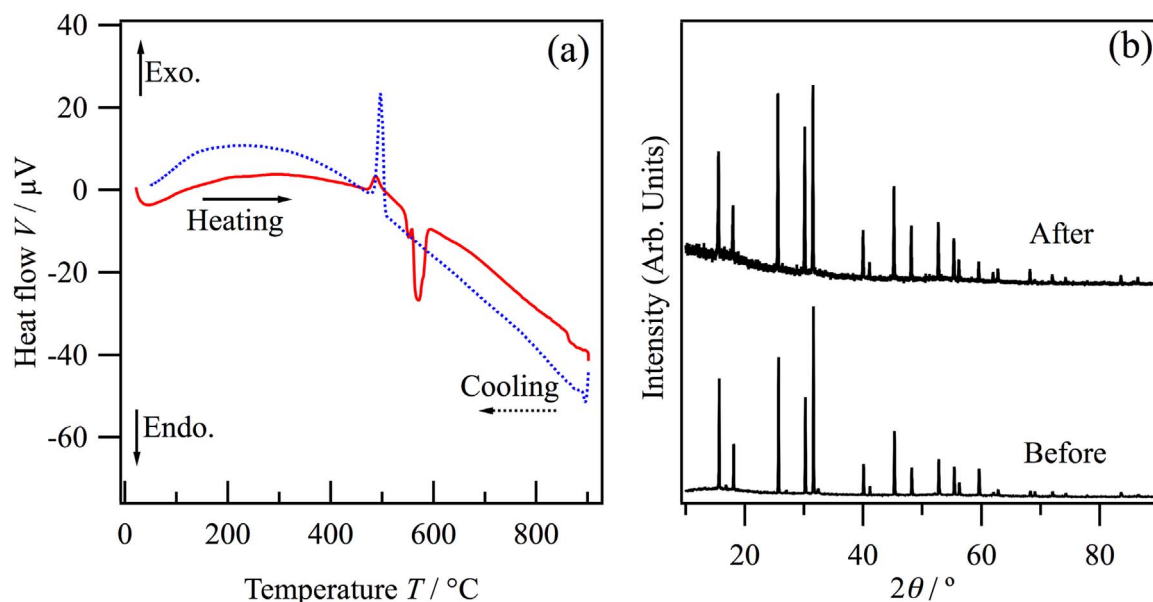
Fig. 7. (a) DTA curves of Li$_7$Ge$_3$PS$_{12}$ sealed in an evacuated quartz ampule, and (b) XRD patterns of Li$_7$Ge$_3$PS$_{12}$ before and after DTA measurements.
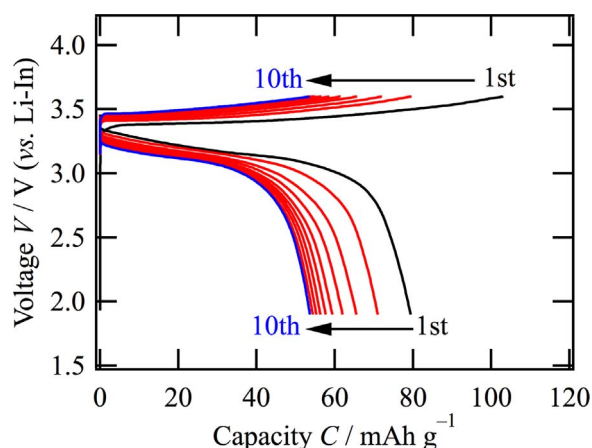

Fig. 8. Charge/discharge curves of the all solid-state battery using Li$_7$Ge$_3$PS$_{12}$, Li-In, and LiNbO$_3$-coated LiCoO$_2$/Li$_{10}$GeP$_2$S$_{12}$ as the electrolyte, anode, and cathode materials, respectively.

a sulfide-based electrolyte [29]. Furthermore, although the capacity decreased following the 1st cycle, we expect that the cycling characteristics can be improved by optimization of the mixing and processing conditions employed during cell fabrication [17]. Thus, the above results indicate that Li$_7$Ge$_3$PS$_{12}$ is a potential candidate for use as a solid electrolyte in all-solid-state batteries.

4. Conclusions

Novel lithium-ion conducting solids were identified within the quasi-ternary Li$_2$S–GeS$_2$–P$_2$S$_5$ system, and the cubic argyrodite-type Li$_7$Ge$_3$PS$_{12}$ was identified as a possible material for application as a solid electrolyte in all-solid-state batteries. The crystal structure of this material was found to contain isolated (Ge/P)S$_4$ tetrahedra, which formed the framework structure, with Li and Ge being distributed in the three-dimensional channels within the assembly. This material exhibited a high ionic conductivity of 1.1×10^{-4} S cm^{-1} at 25 °C and a low activation energy of 25 kJ mol^{-1}, in addition to demonstrating phase stability up to 400 °C. We therefore expect that the discovery of this novel material and its relatively high ionic conductivity will aid in the design of superior lithium-ion conductors exhibiting the argyrodite-type structure. Future studies will focus on elucidation of the phase

relationships in the low- and high-temperature phases of this material. Finally, use of neutron diffraction studies to determine the cation distribution within the structure is expected to allow elucidation of the ionic conduction mechanism of Li$_7$Ge$_3$PS$_{12}$.

Acknowledgements

References

[1] N. Kamaya, K. Homma, Y. Yamakawa, M. Hirayama, R. Kanno, M. Yonemura, T. Kamiyama, Y. Kato, S. Hama, K. Kawamoto, A. Mitsui, A lithium superionic conductor, Nat. Mater. 10 (2011) 682–686.

[2] Y. Kato, S. Hori, T. Saito, K. Suzuki, M. Hirayama, A. Mitsui, M. Yonemura, H. Iba, R. Kanno, High-power all-solid-state batteries using sulfide superionic conductors, Nat, Energy 1 (2016) 16030.

[3] K. Suzuki, M. Sakuma, S. Hori, T. Nakazawa, M. Nagao, M. Yonemura, M. Hirayama, R. Kanno, Synthesis, structure, and electrochemical properties of crystalline Li–P–S–O solid electrolytes: novel lithium-conducting oxysulfides of Li$_{10}$GeP$_2$S$_{12}$ family, Solid State Ion. 288 (2016) 229–234.

[4] A. Hayashi, H. Muramatsu, T. Ohtomo, S. Hama, M. Tatsumisago, Improved chemical stability and cyclability in Li$_2$S–P$_2$S$_5$–P$_2$O$_5$–ZnO composite electrolytes for all-solid-state rechargeable lithium batteries, J. Alloy. Compd. 591 (2014) 247–250.

[5] T. Ohtomo, A. Hayashi, M. Tatsumisago, K. Kawamoto, Characteristics of the Li$_2$O–Li$_2$S–P$_2$S$_5$ glasses synthesized by the two-step mechanical milling, J. Non-Cryst. Solids 364 (2013) 57–61.

[6] R. Kanno, M. Murayama, Lithium ionic conductor thio-LISICON: the Li$_2$–GeS$_2$–P$_2$S$_5$ system, J. Electrochem. Soc. 148 (2001) A742–A746.

[7] S. Hori, M. Kato, K. Suzuki, M. Hirayama, Y. Kato, R. Kanno, Phase diagram of the Li$_4$GeS$_4$–Li$_3$PS$_4$ quasi-binary system containing the superionic conductor Li$_{10}$GeP$_2$S$_{12}$, J. Am. Ceram. Soc. 98 (2015) 3352–3360.

[8] H.-J. Deiseroth, J. Maier, K. Weichert, V. Nickel, S.-T. Kong, C. Reiner, Li$_7$PS$_6$ and Li$_6$PS$_5$X (X: Cl, Br, I): possible three-dimensional diffusion pathways for lithium ions and temperature dependence of the ionic conductivity by impedance measurements, Z. Anorg. Allg. Chem. 637 (2011) 1287–1294.

[9] A. Hayashi, S. Hama, H. Morimoto, M. Tatsumisago, T. Minami, High lithium ion conductivity of glass–ceramics derived from mechanically milled glassy powders, Chem. Lett. 30 (2001) 872–873.

[10] F. Mizuno, A. Hayashi, K. Tadanaga, M. Tatsumisago, High lithium ion conducting glass-ceramics in the system Li$_2$S-P$_2$S$_5$, Solid State Ion. 177 (2006) 2721–2725.

[11] W.F. Kuhs, R. Nitsche, K. Scheunemann, The argyrodites—a new family of tetrahedrally close-packed structures, Mater. Res. Bull. 14 (1979) 241–248.

[12] R.B. Beeken, J.J. Garbe, J.M. Gillis, N.R. Petersen, B.W. Podoll, M.R. Stoneman,

Electrical conductivities of the Ag_6PS_5X and the Cu_6PSe_5X (X=Br, I) argyrodites, J. Phys. Chem. Solids 66 (2005) 882–886.

[13] H. Wada, M. Ishii, M. Onoda, M. Tansho, A. Sato, Preparation, crystal structure and silver ionic conductivity of the new compound Ag_8TiS_6, Solid State Ion. 86 (1996) 159–163.

[14] H.-J. Deiseroth, S.-T. Kong, H. Eckert, J. Vannahme, C. Reiner, T. Zaiß, M. Schlosser, Li6PS5X: A Class of crystalline Li-Rich solids with an unusually high Li^+ mobility, Angew. Chem. Int. Ed. 47 (2008) 755–758.

[15] P. Rayavarapu, N. Sharma, V. Peterson, S. Adams, Variation in structure and Li^+-ion migration in argyrodite-type Li_6PS_5X (X = Cl, Br, I) solid electrolytes, J. Solid State Electr. 16 (2012) 1807–1813.

[16] F. Izumi, K. Momma, Three-dimensional visualization in powder diffraction, Solid State Phenom. 130 (2007) 15–20.

[17] W.J. Li, M. Hirayama, K. Suzuki, R. Kanno, Fabrication and electrochemical properties of a $LiCoO_2$ and $Li_{10}GeP_2S_{12}$ composite electrode for use in all-solid-state batteries, Solid State Ion. 285 (2016) 136–142.

[18] M. Murayama, N. Sonoyama, A. Yamada, R. Kanno, Material design of new lithium ionic conductor, thio-LISICON, in the $Li_2S–P_2S_5$ system, Solid State Ion. 170 (2004) 173–180.

[19] M. Murayama, R. Kanno, Y. Kawamoto, T. Kamiyama, Structure of the thio-LISICON, Li_4GeS_4, Solid State Ion. 154–155 (2002) 789–794.

[20] Y. Matsushita, G.M. Kanatzidis, Synthesis and structure of Li_4GeS_4, Z. Naturforsch. B, J. Chem. Sci. 53 (1998) 23–30.

[21] R. Kanno, T. Hata, Y. Kawamoto, M. Irie, Synthesis of a new lithium ionic conductor, thio-LISICON-lithium germanium sulfide system, Solid State Ion. 130 (2000) 97–104.

[22] J.H. MacNeil, D.M. Massi, J.-H. Zhang, K.A. Rosmus, C.D. Brunetta, T.A. Gentile, J.A. Aitken, Synthesis, structure, physicochemical characterization and electronic structure of thio-lithium super ionic conductors, $Li4_GeS4$ and $Li4_SnS4$, J. Alloy. Compd. 586 (2014) 736–744.

[23] O.Kwon, M.Hirayama, K.Suzuki, Y.Kato, T.Saito, M.Yonemura, T.Kamiyama, R. Kanno, Synthesis, structure, and conduction mechanism of the lithium superionic conductor $Li_{10+d}Ge_{1+d}P_{2-d}S_{12}$, J. Mater. Chem. A3 (2015) 438–446.

[24] J.L. Souquet, E. Robinel, B. Barrau, M. Ribes, Glass formation and ionic conduction in the $M_2S–GeS_2$ (M = Li, Na, Ag) systems, Solid State Ion. 3 (1981) 317–321.

[25] K. Minami, A. Hayashi, M. Tatsumisago, Preparation and characterization of lithium ion conducting $Li_2S–P_2S_5–GeS_2$ glasses and glass-ceramics, J. Non-Cryst. Solids 356 (2010) 2666–2669.

[26] R. Mercier, J.P. Malugani, B. Fahys, J. Douglande, G. Robert, Synthese, structure cristalline et analyse vibrationnelle de l'hexathiohypodiphosphate de lithium $Li_4P_2S_6$, J. Solid State Chem. 43 (1982) 151–162.

[27] S.T. Kong, Ö. Gün, B. Koch, H.J. Deiseroth, H. Eckert, C. Reiner, Structural characterisation of the Li argyrodites Li_7PS_6 and Li_7PSe_6 and their solid solutions: quantification of site preferences by MAS-NMR, Spectrosc. Chem. -Eur. J. 16 (2010) 5138–5147.

[28] Z.D. Hood, C. Kates, M. Kirkham, S. Adhikari, C. Liang, N.A.W. Holzwarth, Structural and electrolyte properties of $Li_4P_2S_6$, Solid State Ion. 284 (2016) 61–70.

[29] Y. Sun, K. Suzuki, K. Hara, S. Hori, T.-A. Yano, M. Hara, M. Hirayama, R. Kanno, Oxygen substitution effects in $Li_{10}GeP_2S_{12}$ solid electrolyte, J. Power Sources 324 (2016) 798–803.